# Learning-aided Collaborative Optimization of Power, Hydrogen, and Transportation Networks

Sheng Chen, Hao Cheng, Si Lv, Zhinong Wei, Peiyue Li, and Jiahui Jin

***Abstract*—The gradual replacement of gasoline vehicles with electric vehicles (EVs) and hydrogen fuel cell vehicles (HFCVs) in recent years has provided a growing incentive for the collaborative optimization of power distribution network (PDN), urban transportation network (UTN), and hydrogen distribution network (HDN). However, an appropriate collaborative optimization framework that addresses the prevalent privacy concerns has yet to be developed, and a sufficient pool of system operators that can competently operate all three networks has yet to be obtained. This study proposes a differentiated taxation-subsidy mechanism for UTNs, utilizing congestion tolls and subsidies to guide the independent traffic flow of EVs and HFCVs. An integrated optimization model for this power-hydrogen-transportation network is established by treating these vehicles and the electrolysis equipment as coupling bridges. We then develop a learning-aided decoupling approach to determine the values of the coupling variables acting among the three networks to ensure the economic feasibility of collaborative optimization. This approach effectively decouples the network, allowing it to operate and be optimized independently. The results for a numerical simulation of a coupled system composed of a IEEE 33-node power network, 13-node Nguyen-Dupuis transportation network, and 20-node HDN demonstrate that the proposed learning-aided approach provides nearly equivalent dispatching results as those derived from direct solution of the physical models of the coupled system, while significantly improving the computational efficiency.**

***Index Terms*—Power-hydrogen-transportation network, collaborative optimization, operational independence, learning-aided decoupling.**

## NOMENCLATURE

### A. Sets

| | |
|---|---|
| $\pi(i)$ | Set of child buses for bus $i$ |
| $\Psi_m^L$ | Set of hydrogen demands connected to node $m$ |
| $\Psi_m^H$ | Set of hydrogen refueling stations (HRSs) connected to node $m$ |
| $\Psi_m^S$ | Set of hydrogen sources connected to node $m$ |
| $\Psi_m^P$ | Set of electrolytic tanks connected to node $m$ |
| $C_e(i)$ | Set of charging links powered by bus $i$ |
| $C_h(i)$ | Set of electrolytic tanks powered by bus $i$ |
| $E_N$ | Set of buses in power distribution network (PDN) |
| $E_L$ | Set of transmission lines in PDN |
| $G(m)$ | Set of hydrogen pipelines connected to node $m$ |
| $K_{rs}^e, K_{rs}^h$ | Sets of electric vehicle (EV) and hydrogen fuel cell vehicle (HFCV) paths connecting an origin-destination (O-D) pair $rs$ |
| $P(m)$ | Set of hydrogen compressors connected to node $m$ |
| $T_N$ | Set of nodes in urban transportation network (UTN) |
| $T_R$ | Set of origin nodes, $T_R \subseteq T_N$ |
| $T_S$ | Set of destination nodes, $T_S \subseteq T_N$ |
| $T_{RS}$ | Set of O-D pairs |
| $T_A^{rg}$ | Set of regular links in UTN |
| $T_A^{ch}$ | Set of charging links in UTN |
| $T_A^{hr}$ | Set of hydrogen refueling links in UTN |

### B. Parameters

| | |
|---|---|
| $\lambda_a^e$ | Charging price at charging station (CS) |
| $\lambda_a^h$ | Hydrogen refueling price at HRS |
| $\xi$ | Power-to-hydrogen (P2H) conversion coefficient |
| $\pi^e, \pi^h$ | Ratios of EV and HFCV traffic demands |
| $\pi_m^f, \pi_m^r$ | Lower and upper limits of hydrogen pressure at node $m$ |
| $\rho$ | Hydrogen gas density |
| $\sigma_p^{Cf}, \sigma_p^{Cr}$ | Lower and upper ratio limits of hydrogen compressor $p$ |
| $\omega$ | Monetary cost of travel time |
| $b_i$ | Energy production cost coefficient of distributed generation (DG) |
| $c_a^{rg}$ | Traffic flow capacity of link $a \in T_A^{rg}$ |
| $c_a^{ch}$ | The maximum allowable vehicular flow of charging link $a \in T_A^{ch}$ |
| $c_a^{hr}$ | The maximum allowable vehicular flow of hydrogen refueling link $a \in T_A^{hr}$ |
| $c_w^S$ | Production cost of hydrogen source $w \in \Psi_m^S$ |

Manuscript received: May 30, 2024; revised: August 6, 2024; accepted: August 28, 2024. Date of CrossCheck: August 28, 2024. Date of online publication: November 27, 2024.



This work was supported by Natural Science Foundation of China (No. 52377091) and Young Elite Scientist Sponsorship Program by CAST (No. 2021QNRC001).

S. Chen (corresponding author), H. Cheng, S. Lv, Z. Wei, P. Li, and J. Jin are with the School of Electrical and Power Engineering, Hohai University, Nanjing 210098, China (e-mail: chenshenghhu@163. com; ch19952880650@163. com; woailanqiust@163. com; wznnj@263. net; 230206030014@hhu. edu. cn; 230206030007@hhu.edu.cn).

DOI: 10.35833/MPCE.2024.000563

$C_{mn}$ Weymouth constant of hydrogen pipeline $mn \in G(m)$

$E_e$ Charging demand of unit traffic flow

$F_p^{Cr}$ Capacity of hydrogen compressor $p \in P(m)$

$F_w^{Sr}$ The maximum production of hydrogen source $w \in \Psi_m^S$

$F_\tau^{\mathrm{P2Hr}}$ Capacity of electrolytic tank $\tau \in \Psi_m^P$

$H_h$ Hydrogen refueling demand of unit traffic flow

$i_l^r$ Square of current flow capacity of line $l \in E_L$

$p_i^{gf}, p_i^{gr}$ Lower and upper limits for active generation of DG at bus $i$

$q_i^{gf}, q_i^{gr}$ Lower and upper limits for reactive generation of DG at bus $i$

$q_{rs}$ Traffic demand between O-D pair $rs$

$t_a^0$ Travel time with free flow on regular link $a \in T_A^{rg}$

$t_a^{c0}$ Travel time with free flow on charging link $a \in T_A^{ch}$

$t_a^{h0}$ Travel time with free flow on hydrogen refueling link $a \in T_A^{hr}$

$U_i^f, U_i^r$ Lower and upper bounds of squared voltage magnitude at bus $i$

$v$ Electricity price of main grid

$V_0$ Voltage magnitude at slack bus

### C. Variables

$\delta_{a,k,rs}^{rg}$ Binary term: if path $k \in K_{rs}^e \bigcup K_{rs}^h$ passes link $a \in T_A^{rg}$, $\delta_{a,k,rs}^{rg} = 1$; otherwise, $\delta_{a,k,rs}^{rg} = 0$

$\delta_{a,k,rs}^{e}$ Binary term: if path $k \in K_{rs}^e$ passes link $a \in T_A^{ch}$, $\delta_{a,k,rs}^{e} = 1$; otherwise, $\delta_{a,k,rs}^{e} = 0$

$\delta_{a,k,rs}^{h}$ Binary term: if path $k \in K_{rs}^h$ passes link $a \in T_A^{hr}$, $\delta_{a,k,rs}^{h} = 1$; otherwise, $\delta_{a,k,rs}^{h} = 0$

$\theta_p$ Energy conversion efficiency of hydrogen compressor $p$

$\pi_m$ Hydrogen pressure at node $m$

$\pi_p^{in}, \pi_p^{out}$ Hydrogen pressures of compressor $p \in P(m)$ at inlet and outlet

$c_{k,rs}^e$ EV travel cost on path $k \in K_{rs}^e$ between O-D pair $rs$

$c_{k,rs}^h$ HFCV travel cost on path $k \in K_{rs}^h$ between O-D pair $rs$

$f_{k,rs}^e$ EV flow on path $k \in K_{rs}^e$ between O-D pair $rs$

$f_{k,rs}^h$ HFCV flow on path $k \in K_{rs}^h$ between O-D pair $rs$

$Fee_a^e$ Charging service fee on link $a \in T_A^{ch}$

$Fee_a^{hr}$ Hydrogen refueling service fee on link $a \in T_A^{hr}$

$F_e^L$ Amount of hydrogen demand $e \in \Psi_m^L$ consumed

$F_a^h$ Hydrogen consumption of HRSs on link $a \in T_A^{hr}$

$\overline{F_a^h}$ Predicted hydrogen consumption of HRSs on link $a \in T_A^{hr}$

$F_w^S$ Hydrogen production of hydrogen source $w \in \Psi_m^S$

$F_\tau^{\mathrm{P2H}}$ Hydrogen production of electrolytic tank $\tau \in \Psi_m^P$

$\overline{F_\tau^{\mathrm{P2H}}}$ Predicted hydrogen production of electrolytic tank $\tau \in \Psi_m^P$

$F_p^C$ Hydrogen flow through compressor $p \in P(m)$

$F_{mn}$ Hydrogen flow through pipeline $mn$

$i_{ij}^l$ Squared current magnitude of line $l$ from buses $i$ to $j$

$p_i^d$ Active power demand at bus $i$

$p_i^e$ Total charging power demand at bus $i$

$p_i^{reg}$ Regular power demand at bus $i$

$\overline{p_i^e}$ Predicted total charging power demand at bus $i$

$p_i^{\mathrm{P2H}}$ Total power demand for hydrogen production at bus $i$

$\overline{p_i^{\mathrm{P2H}}}$ Predicted total power demand for hydrogen production at bus $i$

$p_i^g$ Generated active power at bus $i$

$P_{ij}^l$ Active power flow of line $l$ from buses $i$ to $j$

$q_i^d$ Reactive power demand at bus $i$

$q_i^g$ Generated reactive power at bus $i$

$Q_{ij}^l$ Reactive power flow of line $l$ from buses $i$ to $j$

$r_{ij}^l$ Resistance of line $l$ from buses $i$ to $j$

$t_a^{rg}$ Travel time on link $a \in T_A^{rg}$

$t_a^{ch}$ Average time spent by EVs on link $a \in T_A^{ch}$

$t_a^{hr}$ Average time spent by HFCVs on link $a \in T_A^{hr}$

$Toll_a^e$ Congestion toll of EVs on link $a \in T_A^{rg}$

$Toll_a^h$ Congestion toll of HFCVs on link $a \in T_A^{rg}$

$u_{rs}^e$ The minimum travel cost of EVs between O-D pair $rs$

$u_{rs}^h$ The minimum travel cost of HFCVs between O-D pair $rs$

$U_i$ Squared voltage magnitude at bus $i$

$x_a^{rg}$ Aggregated traffic flow on link $a \in T_A^{rg}$

$x_a^{ch}$ Aggregated EV flow on link $a \in T_A^{ch}$

$\overline{x_a^{ch}}$ Predicted aggregated EV flow on link $a \in T_A^{ch}$

$x_a^{hr}$ Aggregated HFCV traffic flow on link $a \in T_A^{hr}$

$\overline{x_a^{hr}}$ Predicted aggregated HFCV traffic flow on link $a \in T_A^{hr}$

$x_{ij}^l$ Reactance of line $l$ from buses $i$ to $j$

$z_{ij}^l$ Impedance of line $l$ from buses $i$ to $j$, $(z_{ij}^l)^2 = (r_{ij}^l)^2 + (x_{ij}^l)^2$

## I. Introduction

To effectively reduce the carbon emissions within the transportation sector, the global transition toward renewable energy sources has promoted the increasing use of new energy vehicles [1]. Of these, electric vehicles (EVs) have been a subject of considerable interest [2]. However, due to the advancement of power-to-hydrogen (P2H) technologies [3], the promotion of green hydrogen production technologies, and the anticipated reduction in hydrogen costs in the foreseeable future, hydrogen fuel cell vehicles (HFCVs),

which are often overlooked, hold promising developmental prospects [4]. These prospects have motivated several governments to foster the development of HFCVs.

The increased presence of charging stations (CSs) and EVs has significantly enhanced the coupling between power distribution networks (PDNs) and urban transportation networks (UTNs) [5]. This also applies to the coupling between hydrogen distribution networks (HDNs) and UTNs under the increasing implementation of hydrogen refueling stations (HRSs) and HFCVs [6]. Increasing the penetration of renewable energy generation would also strengthen the interactions between PDNs and UTNs because reducing the production cost of hydrogen would increase the implementation of HFCVs [7]. These conditions provide a growing incentive for the collaborative optimization of PDNs, HDNs, and UTNs via approaches considering the significant operational challenges involved. For example, these three networks are operated by different entities that must be responsive to prevalent information privacy concerns.

Existing studies have primarily focused on the coordinated optimization of PDNs and UTNs while considering EVs. For example, [8] proposed a hybrid economic-emission dispatch model that employs a differentiated pricing scheme and an accuracy-aware adaptive piecewise linearization method to coordinate the operations of PDNs and UTNs. Reference [9] proposed a novel collaborative pricing scheme for coupled PDNs and UTNs using a variational inequality approach, where the operational cost is effectively minimized through coordinated nodal electricity prices and congestion tolls. Reference [10] developed a decentralized bi-level decomposition method to optimize the operation of EVs in coupled UTN and PDN, thereby effectively managing power-traffic flows while preserving network data privacy. Reference [11] introduced a novel bi-level optimal scheduling framework to coordinate the operation schedules of electric bus fleets and integrate the dispatch of heterogeneous energy resources into a regional integrated energy system. Reference [12] proposed a method for the service restoration of distribution networks using transportable power sources and repair crews, employing a two-stage stochastic program and a two-phase scenario reduction method for efficient solution.

In terms of the efforts to achieve coordinated optimization of HDNs with UTNs and PDNs when considering HFCVs, [13] achieved efficient resource allocation for coupled HDNs and UTNs by applying the demand response of HFCV users, and [14] proposed a coordinated planning strategy for PDNs and HDNs with hydrogen supply chains. Compared with systems that operate in isolation, this strategy was shown to enhance the flexibility and reliability of the combined system by taking advantage of the synergistic effects and coupling relationships of the two networks.

The learning-aided approaches have also been extensively employed to coordinate the operations of PDN and UTN. For example, [15] proposed a mobility-aware charging scheduling approach for a shared EV fleet using deep reinforcement learning combined with binary linear programming. Reference [16] developed a dynamic pricing framework for CSs using a customized deep reinforcement learning approach to maximize the quality of service at a differentiated service requirement level. Reference [17] presented a multi-agent deep reinforcement learning approach to model and optimize the pricing game of CSs in a UTN. Reference [18] proposed a novel deep learning based surrogate modeling method that combined an edge-conditioned convolutional network and a deep belief network to accurately map the spatial dependencies and uncertainties in EV user equilibrium (UE). Reference [19] developed a dynamic pricing strategy for fast-charging CSs using deep reinforcement learning. A prediction method was applied to determine the charging demand distributions, and an EV satisfaction model was applied to make charging decisions. Reference [20] proposed a transfer learning method based on deep reinforcement learning for developing an EV charging strategy in new environments. The accurate policy evaluation was achieved by adding a critic network to the target task and utilizing a Markov decision process to describe the EV charging control model. Reference [21] developed a deep reinforcement learning approach to minimize the travel time and charging costs of EV users navigating to CSs by coordinating the operations of intelligent UTNs. Reference [22] proposed a multi-agent deep reinforcement learning approach with centralized training for scheduling decentralized EV charging operations in a smart grid, and its effectiveness in minimizing operational costs was demonstrated. The complex problem of coordinating the operations of PDNs, HDNs, and UTNs in conjunction with HFCVs was addressed by [23], which utilized deep reinforcement learning to determine the optimal hydrogen refueling price.

Although many studies have investigated collaborative optimization of the operations of PDN, HDN, and UTN, the efforts to coordinate the operations of these networks still have two major limitations.

1) As previously discussed, limited attention has been directed toward the coordinated optimization of HDNs while considering HFCVs. An appropriate collaborative optimization framework for power-hydrogen-transportation networks that fully addresses privacy concerns has yet to be developed. In addition, the computational efficiency of an integrated optimization model for PDN, HDN, and UTN is insufficient to satisfy real-world scheduling demands. However, directly employing a data-driven approach to produce the collaborative optimization results of a power-hydrogen-transportation network often violates physical constraints such as voltage constraints.

2) Because PDNs, HDNs, and UTNs are operated by different entities, significant operational challenges are greatly exacerbated by the absence of a single operator that can competently operate all three networks. This challenge is compounded by the implementation of distributed dispatch algorithms, as this condition can produce numerous secondary issues such as significant increases in communication time, computational delays, and convergence problems due to the non-convexity of energy flow models.

This paper addresses these limitations by proposing a learning-aided collaborative optimization framework for an integrated power-hydrogen-transportation network that en-

sures the economic feasibility of collaborative operations. Accordingly, this paper makes the following contributions.

1) The proposed collaborative optimization framework considers the constraints of the PDN, HDN, and UTN individually. This framework incorporates coupling constraints between ① the PDN and UTN with respect to the charging activities of EV users, ② the HDN and UTN with respect to the refueling activities of HFCV users, and ③ the PDN and HDN with respect to P2H units. We also introduce a differentiated taxation-subsidy mechanism for UTN that guides vehicles toward less congested routes by imposing congestion tolls on regular links and encourages users to consume renewable energy via subsidies at CSs and HRSs. The congestion tolls and subsidies are tailored specifically for EVs and HFCVs. This mechanism enhances the flexibility of UTN management to improve the traffic dispatch efficiency. It also prevents the "collective punishment" phenomenon in vehicle scheduling and ensures that the UTN operates efficiently with the PDN and HDN, thereby reducing the overall operational costs of the three networks.

2) The proposed learning-aided approach employs a model-free deep neural network (DNN) framework to determine the optimal values of the coupling variables acting between the three networks. These optimal values are then applied to decouple the network for independent operation. This greatly simplifies the optimization process, restricts the exchange of private information between the three network operators, and eliminates the need for operators to have specific information about the operations of all three networks. Therefore, the proposed learning-aided approach aligns with the operational independence of each network while simultaneously showcasing the merits of collaborative coordination.

3) The results of numerical computations demonstrate that the proposed learning-aided approach provides dispatching results that are nearly equivalent to those obtained by directly solving the physical models of the coupled system. The proposed learning-aided approach also reduces the required computation time by 96%. We also clarify the potential for PDNs and HDNs integrated with P2H units to accommodate renewable energy generation based on the energy consumption of EVs and HFCVs, respectively.

The remainder of this paper is organized as follows. Section II presents the coupling relationships in a typical power-hydrogen-transportation network, i.e., the combined system with PDN, HDN, and UTN. These relationships are then included with the mathematical formulations of the UTN, HDN, and PDN to establish a collaborative optimization model. Section III presents the DNN architecture of the proposed learning-aided approach and individual optimization models applied to each network following decoupling via the DNN. Section IV presents the results of a numerical simulation of an IEEE 33-node power network, 13-node Nguyen-Dupuis transportation network, and 20-node HDN. Section V concludes this study.

## II. Power-Hydrogen-Transportation Network Model

Figure 1 illustrates the coupling relationships in a typical combined system with PDN, HDN, and UTN. Here, CSs, HRSs, and P2H units (i.e., electrolyzers) act as bridges connecting the operations of the three networks together, where EV charging via CSs in the UTN requires electricity from the PDN, the refueling of HFCVs via HRSs in the UTN requires hydrogen supply from the HDN, and the operation of P2H units requires electricity from the PDN to generate hydrogen for the HDN. In addition, the traffic flows of EVs and HFCVs dictate the electricity and hydrogen demands of the CSs and HRSs, respectively. This study considers both EVs and HFCVs, as they play a dominant and strategically important role in the transition to a sustainable energy future. This choice is also driven by the expected integration of renewable energy and decarbonization in the transportation sector.

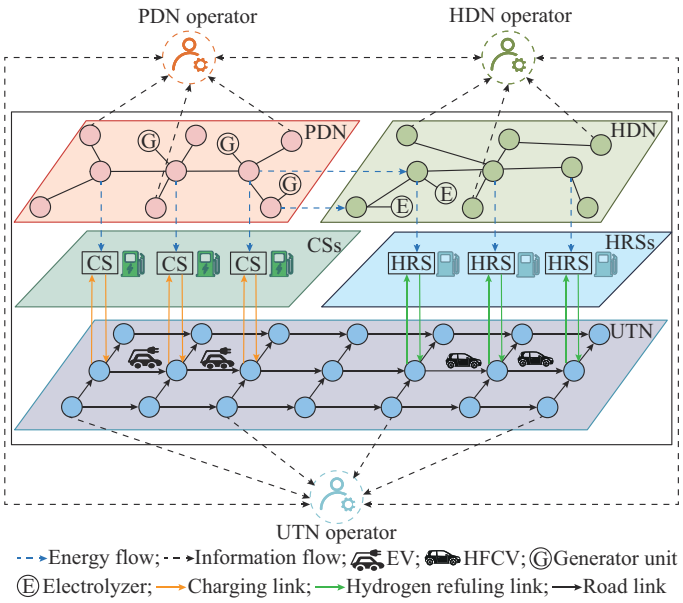


Fig. 1. Coupling relationships in a typical combined system with PDN, HDN, and UTN.

### A. UTN Modeling

As illustrated in Fig. 2, the coupling among the three networks is facilitated by categorizing four types of transportation links in the UTN: regular, charging, hydrogen refueling, and bypass links. Regular links refer to physical connections between individual roadways. Charging, hydrogen refueling, and bypass links are conceptual connections, where charging links correspond to the queuing and charging events of EVs at CSs, hydrogen refueling links correspond to the queuing and refueling events of HFCVs at HRSs, and bypass links depict events involving EVs/HFCVs bypassing CSs/HRSs. We assume a static traffic assignment model in which the traffic conditions and network parameters remain constant. This model implicitly assumes perfect rationality among drivers who seek the most efficient routes to minimize their travel costs, including time, charging, and refueling expenses. Although the models of EVs and HFCVs in the UTN are similar, EVs primarily serve the coupling of the UTN and PDN, whereas HFCVs mainly serve the coupling of the UTN and HDN. Therefore, it is necessary to design differentiated pricing mechanisms to provide guidances while prevent the "collective punishment" effect.

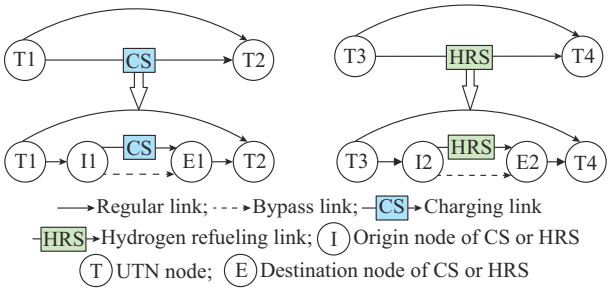


Fig. 2. Schematic illustrating four types of transportation links applied in UTN.

For the UTN, the mixed UE conditions between EVs and HFCVs can be modeled as follows [24].

*1) Traffic Flow Constraints*

$$\pi^e q_{rs} = \sum_{k \in K^e_{rs}} f^e_{k,rs} \tag{1}$$

$$\pi^h q_{rs} = \sum_{k \in K^h_{rs}} f^h_{k,rs} \tag{2}$$

$$x^{rg}_a = \sum_{rs} \sum_{k \in K^e_{rs}} f^e_{k,rs} \delta^{rg}_{a,k,rs} + \sum_{rs} \sum_{k \in K^h_{rs}} f^h_{k,rs} \delta^{rg}_{a,k,rs} \quad a \in T^{rg}_A \tag{3}$$

$$x^{ch}_a = \sum_{rs} \sum_{k \in K^e_{rs}} f^e_{k,rs} \delta^e_{a,k,rs} \quad a \in T^{ch}_A \tag{4}$$

$$x^{hr}_a = \sum_{rs} \sum_{k \in K^h_{rs}} f^h_{k,rs} \delta^h_{a,k,rs} \quad a \in T^{hr}_A \tag{5}$$

Here, (1) and (2) describe the relationships between traffic demands and traffic flows on paths, and (3)-(5) describe the relationship between traffic flows on links and paths.

*2) Travel Time Constraints*

For regular links, we correlate the travel time and traffic flow according to the function of the Bureau of Public Roads as:

$$t^{rg}_a = t^0_a \left(1 + 0.15 \left(\frac{x^g_a}{c^{rg}_a}\right)^4\right) \quad a \in T^{rg}_A \tag{6}$$

For charging and hydrogen refueling links, the queuing time of EVs and HFCVs at the CSs and HRSs is defined as (7) and (8), respectively, according to the Davidson model.

$$t^{ch}_a = t^{c0}_a \left(1 + J \frac{x^{ch}_a}{c^{ch}_a - x^{ch}_a}\right) \quad x^{ch}_a < c^{ch}_a, a \in T^{ch}_A \tag{7}$$

$$t^{hr}_a = t^{h0}_a \left(1 + J \frac{x^{hr}_a}{c^{hr}_a - x^{hr}_a}\right) \quad x^{hr}_a < c^{hr}_a, a \in T^{hr}_A \tag{8}$$

where $J$ is typically set to be 0.05.

*3) Travel Cost Constraints*

The travel costs for EVs and HFCVs are defined as:

$$c^e_{k,rs} = \sum_{a \in T^{rg}_A} (\omega t^{rg}_a + Toll^e_a) \delta^e_{a,k,rs} + \sum_{a \in T^{ch}_A} (\omega t^{ch}_a + \lambda^e_a E_e - Fee^e_a) \delta^e_{a,k,rs} \tag{9}$$

$$c^h_{k,rs} = \sum_{a \in T^{rg}_A} (\omega t^{rg}_a + Toll^h_a) \delta^h_{a,k,rs} + \sum_{a \in T^{hr}_A} (\omega t^{hr}_a + \lambda^h_a H_h - Fee^{hr}_a) \delta^h_{a,k,rs} \tag{10}$$

As can be seen, the overall travel costs are the sum of the travel costs on each link and mainly include the time, charging, hydrogen refueling, and response costs to the price regulations of the system operator. We incorporate the response cost from previous studies into the differentiated taxation-subsidy mechanism, guiding users to less-congested road links by imposing separate congestion tolls on EVs and HFCVs. In addition, subsidies are provided at CSs and HRSs to attract EVs and HFCVs to stations with shorter queues or higher renewable energy availability. This pricing mechanism effectively mitigates the traffic congestion and reduces travel costs.

*4) UE Constraints*

The UE constraints for the traffic flow on path $k$ between origin-destination (O-D) pair $rs$ are based on Wardrop's first principle.

$$0 \le f^e_{k,rs} \perp c^e_{k,rs} - u^e_{rs} \ge 0 \tag{11}$$

$$0 \le f^h_{k,rs} \perp c^h_{k,rs} - u^h_{rs} \ge 0 \tag{12}$$

This principle posits that a UTN reaches an equilibrium state when all road users are fully aware of network traffic conditions and select the most efficient available routes. Consequently, users cannot further reduce their travel expenditures by modifying their route preferences under UE conditions. Notably, without the incorporation of the differentiated taxation-subsidy mechanism under the UE criterion, EVs and HFCVs can only achieve equilibrium operations in the UTN. In this case, EVs and HFCVs lack sufficient price incentives to alter their routes or choose alternative CSs and HRSs, thereby preventing the UTN from coordinating with the PDN and HDN. By contrast, via the introduction of this novel pricing mechanism, EVs and HFCVs become connecting bridges of the UTN with PDN and HDN.

The UTN constraints include (1)-(12).

## B. HDN Modeling

The steady-state operational constraints of an HDN are analogous to those of a natural gas network and can be expressed as [25]:

$$\sum_{e \in \Psi^L_m} F^L_e + \sum_{a \in \Psi^H_m} F^h_a - \sum_{w \in \Psi^S_m} F^S_w - \sum_{\tau \in \Psi^P_m} F^{\mathrm{P2H}}_\tau + \sum_{p \in P(m)} (1 + \theta_p) F^C_p + \sum_{n \in G(m)} F_{mn} = 0 \tag{13}$$

$$0 \le F^S_w \le F^{Sr}_w \tag{14}$$

$$0 \le F^{\mathrm{P2H}}_\tau \le F^{\mathrm{P2H}r}_\tau \tag{15}$$

$$0 \le F^C_p \le F^{Cr}_p \tag{16}$$

$$\pi^{in}_p \sigma^{Cf}_p \le \pi^{out}_p \le \pi^{in}_p \sigma^{Cr}_p \tag{17}$$

$$F_{mn} \left| F_{mn} \right| / C^2_{mn} = \pi^2_m - \pi^2_n \tag{18}$$

$$\pi^f_m \le \pi_m \le \pi^r_m \tag{19}$$

As (13) shows, all hydrogen demands at node $m$ of the HDN must be balanced. Constraint (14) corresponds to the supply constraint of the gas source $w$, (15) represents the supply constraint of the electrolytic tank $\tau$, (16) and (17) represent the operational constraints of the compressor $p$, (18) describes the nonlinear relationship between the hydrogen flow in the pipeline $mn$ and the pressure values at its inlet

and outlet, and (19) enforces safety constraints on the pressure values at node $m$.

The hydrogen consumption $F_a^h$ of the HRSs on link $a$ represents the coupling between the HDN and UTN, which is defined as:

$$F_a^h = x_a^{hr} H_h / \rho \quad a \in \Psi_m^H \tag{20}$$

Utilizing second-order cone (SOC) relaxation, the nonlinear functional relationship given in (18) can be reformulated as:

$$F_{mn}^2 / C_{mn}^2 \le \pi_m^2 - \pi_n^2 \tag{21}$$

The standardized SOC representation of (21) is given as [26]:

$$\left\| \begin{matrix} F_{mn}/C_{mn} \\ \pi_n \end{matrix} \right\| \le \pi_m \tag{22}$$

The HDN constraints include (13)-(22).

### C. PDN Modeling

A PDN is typically described by a conventional DistFlow model. However, this model includes nonlinear terms that are non-convex and challenging to solve. This issue can be addressed effectively by applying the SOC relaxation technique to the nonlinear terms in the DistFlow model, and we can obtain [27], [28]:

$$P_{ij}^l + p_j^g - r_{ij}^l i_{ij}^l = \sum_{h \in \pi(j)} P_{jh}^l + p_j^d \tag{23}$$

$$Q_{ij}^l + q_j^g - x_{ij}^l i_{ij}^l = \sum_{h \in \pi(j)} Q_{jh}^l + q_j^d \tag{24}$$

$$U_j = U_i - 2(r_{ij}^l P_{ij}^l + x_{ij}^l Q_{ij}^l) + (z_{ij}^l)^2 i_{ij}^l \tag{25}$$

$$i_{ij}^l \ge \frac{(P_{ij}^l)^2 + (Q_{ij}^l)^2}{U_i} \tag{26}$$

$$\begin{cases} i_{ij}^l \le i_l^r \\ U_i^f \le U_i \le U_i^r \end{cases} \tag{27}$$

$$\begin{cases} p_i^{gf} \le p_i^g \le p_i^{gr} \\ q_i^{gf} \le q_i^g \le q_i^{gr} \end{cases} \tag{28}$$

Equations (23) and (24) denote the active and reactive power balances, respectively. Equation (25) establishes a nonlinear Ohm's law relationship between the line voltage and current in the squared form, and (26) represents its corresponding SOC relaxation. Note that the voltage magnitude at the slack bus is constant. Equation (27) imposes the upper and lower bounds on the squared values of the voltage and current amplitudes, and (28) specifies the upper and lower bounds for the active and reactive power outputs of distributed generation (DG) units. The total active power demand is defined as:

$$p_j^d = p_j^{reg} + p_j^e + p_j^{\mathrm{P2H}} \tag{29}$$

where $p_j^e$ signifies the coupling between the PDN and UTN, and $p_i^{\mathrm{P2H}}$ signifies the coupling between the PDN and HDN. The two demand terms can be expressed as:

$$p_j^e = x_a^{ch} E_e \quad a \in C_e(j) \tag{30}$$

$$p_j^{\mathrm{P2H}} = \rho F_\tau^{\mathrm{P2H}} \xi \quad \tau \in C_h(j) \tag{31}$$

The PDN constraints include (23)-(31).

### D. Power-hydrogen-transportation Network Dispatch Model

Under the UE conditions, all routes carrying a positive traffic flow between O-D pair *rs* share the same travel costs. Therefore, the overall travel cost for travelers in UTN can be formulated as:

$$\begin{aligned} F_{UTN}^{eco} = & \sum_{rs} \sum_{k \in K_{rs}^e} c_{k,rs}^e f_{k,rs}^e + \sum_{rs} \sum_{k \in K_{rs}^h} c_{k,rs}^h f_{k,rs}^h = \sum_{rs} u_{rs}^e \sum_{k \in K_{rs}^e} f_{k,rs}^e + \\ & \sum_{rs} u_{rs}^h \sum_{k \in K_{rs}^h} f_{k,rs}^h = \sum_{rs} u_{rs}^e \pi^e q_{rs} + \sum_{rs} u_{rs}^h \pi^h q_{rs} \end{aligned} \tag{32}$$

The economic cost of PDN encompasses both the generation cost of the DG units and the cost of purchasing electricity from the main grid, which is defined as:

$$F_{PDN}^{eco} = \sum_{i \in E_N} b_i p_i^g + v \sum_{j \in \pi(0)} P_{0j}^l \tag{33}$$

The economic cost of HDN is the supply cost of hydrogen sources, which can be formulated as:

$$F_{HDN}^{eco} = \sum_{w \in \Psi_m^S} c_w^S F_w^S \tag{34}$$

Finally, the applied economic optimization model for the power-hydrogen-transportation network is derived by minimizing the sum of the defined economic costs as:

$$\begin{cases} \min F_{eco} = F_{UTN}^{eco} + F_{PDN}^{eco} + F_{HDN}^{eco} \\ \text{s.t. (1)-(31)} \end{cases} \tag{35}$$

## III. Proposed Learning-aided Approach

The proposed collaborative optimization framework ensures the operational independence of the PDN, HDN, and UTN by learning the coupling variables (i.e., EV charging demand, HFCV hydrogen consumption, and power demand for hydrogen production) between them via a learning-aided approach. This approach leverages a DNN to predict the coupling variables, thereby minimizing the need for data sharing and maintaining the confidentiality of operational data in each network. In addition, the model-free architecture of DNN and aggregated anonymized data exchange protect against unauthorized access and potential data breaches. Privacy is further enhanced through strict access control, transparent data usage policies, and regular security audits, all of which contribute to safeguarding sensitive information while allowing for efficient network optimization.

### A. DNN

#### 1) Structure and Learning Goals

In general, DNNs are machine learning models that consist of multiple layers, where each layer takes the outputs from the previous layer as its inputs. In standard feedforward neural networks, each node in one layer is connected to all nodes in the next layer. The function that connects these layers is given by:

$$\boldsymbol{y} = \pi(\boldsymbol{W}\boldsymbol{x} + \boldsymbol{b}) \tag{36}$$

where $\boldsymbol{x} \in \mathbf{R}^N$ and $\boldsymbol{y} \in \mathbf{R}^M$ are the input and output vectors, and $N$ and $M$ are the numbers of demands and coupling variables, respectively; $\boldsymbol{W} \in \mathbf{R}^{M \times N}$ is the weight matrix; $\boldsymbol{b} \in \mathbf{R}^M$ is the bias vector; and $\pi(\cdot)$ is a nonlinear activation function,

and in this paper, a rectified linear unit (ReLU) activation function is applied.

Figure 3 illustrates the architecture of the DNN applied. Specifically, the input of DNN $\boldsymbol{x}$ includes the known traffic, electricity, and hydrogen demands, i.e., $q_{rs}$, $p_i^{reg}$, and $F_e^L$, respectively, and the output of DNN $\boldsymbol{y}$ is the predicted values of the coupling variables, including the hydrogen consumption of HRSs on link $a$, the total charging power demand at bus $i$, and the total electricity demand for hydrogen production at bus $i$, i.e., $\overline{F_a^h}$, $\overline{p_i^e}$, and $\overline{p_i^{\mathrm{P2H}}}$, respectively.

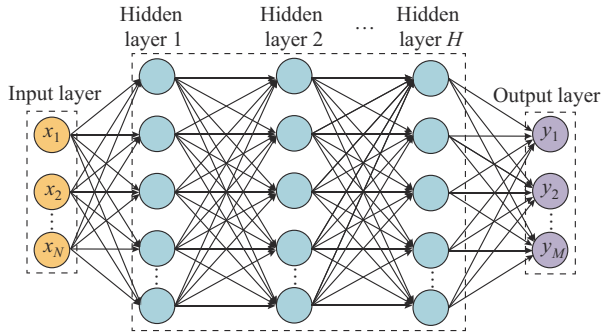


Fig. 3. Architecture of DNN.

Formally, the resulting predictor learns the mapping $O$: $\mathbf{R}^N \rightarrow \mathbf{R}^M$. The input of the learning task is a dataset $D=(x_l, y_l)$, $x_l=(q_{rs}, p_i^{reg}, F_e^L)$ and $y_l=(F_a^h, p_i^e, p_i^{\mathrm{P2H}})$ represent the $l^{\mathrm{th}}$ observations of the demands and coupling variables, respectively, and $y_l=O(x_l)$. The output is a function $\hat{O}$, which ideally represents the outcome of the following optimization problem:

$$\min \sum_l L_o(y_l, \hat{O}(x_l)) \tag{37}$$

where the Huber loss function $L_o$ is expressed as (38), which offers improved robustness over the commonly-used loss functions by effectively reducing the sensitivity to outlier [29].

$$L_o(y_l, \hat{O}(x_l)) = \begin{cases} \dfrac{1}{2}(y_l - \hat{O}(x_l))^2 & \left| y_l - \hat{O}(x_l) \right| \le \delta \\ \delta \left| y_l - \hat{O}(x_l) \right| - \dfrac{1}{2}\delta^2 & \left| y_l - \hat{O}(x_l) \right| > \delta \end{cases} \tag{38}$$

where the parameter $\delta$ is set to be a default value of 1.

In this paper, we use Bayesian search to tune the hyperparameters of DNN, which navigates vast hyperparameter spaces systematically and efficiently by leveraging probabilistic models to pinpoint configurations that maximize the model performance [30]. We apply the open-source Optuna hyperparameter optimization framework, the core of which is an Optuna study object composed of a collection of trial objects that share the same search space and objective function. Accordingly, an initial search space for hyperparameters is first defined, which is followed by iterative trials. For each iteration, a probabilistic model suggests a new hyperparameter combination based on the outcomes of prior trials. The DNN is then trained using the suggested hyperparameters, and its prediction performance is evaluated using the coefficient of determination $R^2$ to reflect the fitting performance of the trained DNN, which achieves a maximum performance at $R^2=1.0$. This iterative process refines the search and ultimately yields a hyperparameter combination that maximizes the $R^2$ value. Note that the coupling relationships between the three networks are more complex in reality. For simplicity, we focus on the learning-aided decoupling of three typical coupling variables. The main challenges in the practical implementation of the proposed collaborative optimization framework include ensuring high-quality real-time data acquisition, managing computational complexity for large-scale network optimization, generalizing the DNN model across diverse operational scenarios, integrating with existing infrastructure, navigating regulatory diversity, aligning economic incentives for stakeholders, and achieving user acceptance.

### *B. Decoupled Optimization of Power-hydrogen-transportation Network*

As previously discussed, the optimal values of the coupling variables between the three networks are predicted by the DNN, and these predicted values are applied to decouple these networks. Accordingly, we first replace $F_a^h$ in (13) with the predicted value $\overline{F_a^h}$ and replace $p_i^e$ and $p_i^{\mathrm{P2H}}$ in (29) with the predicted values $\overline{p_i^e}$ and $\overline{p_i^{\mathrm{P2H}}}$, respectively. From (31), we can deduce $\overline{F_\tau^{\mathrm{P2H}}}$ as:

$$\overline{F_\tau^{\mathrm{P2H}}} = \frac{\overline{p_j^{\mathrm{P2H}}}}{\rho\xi} \quad \tau \in C_h(j) \tag{39}$$

Thus, (13) can be transformed into (40) with predicted values:

$$\sum_{e \in \Psi_m^L} F_e^L + \sum_{a \in \Psi_m^H} \overline{F_a^h} - \sum_{w \in \Psi_m^S} F_w^S - \sum_{\tau \in \Psi_m^P} \overline{F_\tau^{\mathrm{P2H}}} + \sum_{p \in P(m)} (1+\theta_p) F_p^C + \sum_{n \in G(m)} F_{mn} = 0 \tag{40}$$

The newly obtained HDN constraints include (15) - (21), (39), and (40). The decoupled HDN model can be described succinctly as:

$$\begin{cases} \min F_{eco} = F_{HDN}^{eco} \\ \text{s.t. (15)-(21), (39), (40)} \end{cases} \tag{41}$$

Similarly, (29) is transformed into:

$$p_j^d = p_j^{reg} + \overline{p_j^e} + \overline{p_j^{\mathrm{P2H}}} \tag{42}$$

The newly obtained PDN constraints include (23) - (28), (42). The decoupled PDN model can be expressed succinctly as:

$$\begin{cases} \min F_{eco} = F_{PDN}^{eco} \\ \text{s.t. (23)-(28), (41)} \end{cases} \tag{43}$$

To decouple the UTN, the power demand and hydrogen consumption values predicted by the DNN for the PDN and HDN essentially represent the predicted distributions of the EVs and HFCVs at the CSs and HRSs, respectively. Based on (20) and (30), the flow distributions of EVs and HFCVs can be expressed as:

$$\overline{x_a^{ch}} = \frac{\overline{p_j^e}}{E_e} \quad a \in C_e(j) \tag{44}$$

$$\overline{x_a^{hr}} = \frac{\overline{F_a^h}\rho}{H_h} \quad a \in \Psi_m^H \tag{45}$$

In addition, (7) and (8) can be transformed into:

$$t_a^{ch} = t_a^{c0}\left(1 + J\frac{\overline{x_a^{ch}}}{c_a^{ch} - \overline{x_a^{ch}}}\right) \quad a \in T_A^{ch} \tag{46}$$

$$t_a^{hr} = t_a^{h0}\left(1 + J\frac{\overline{x_a^{hr}}}{c_a^{hr} - \overline{x_a^{hr}}}\right) \quad a \in T_A^{hr} \tag{47}$$

The newly obtained UTN constraints include (1)-(3), (6), (9)-(12), and (44)-(47). The decoupled UTN model can be described succinctly as:

$$\begin{cases} \min F_{eco} = F_{UTN}^{eco} \\ \text{s.t. (1)-(3), (6), (9)-(12), (44)-(47)} \end{cases} \tag{48}$$

In the real world, the application of proposed learning-aided approach may encounter regulatory and policy challenges. It is imperative to harmonize regulations across various departments to ensure cohesive and effective policy implementation. In addition, the stringent adherence to data privacy regulations is essential to safeguard the sensitive information of individuals and organizations.

Furthermore, structural reforms are needed. Market structures must be reconfigured to incentivize participation by all relevant stakeholders. Concurrently, the integration of supporting technologies is critical, where the establishment of requisite infrastructure and systems is required to facilitate the implementation of the proposed learning-aided approach.

The role of the predictor can be fulfilled by specialized agencies or departments within existing utility companies that already perform data analysis and forecasting tasks. These entities are well-equipped with the necessary expertise and infrastructure to extend their services to the proposed collaborative optimization framework.

## IV. Case Study

Figure 4 shows the coupled system composed of IEEE 33-node power network [31], 13-node Nguyen-Dupuis transportation network [32], and 20-node HDN [33]. Other details of the test system are available in Supplementary Material A. All computational analyses are performed on a laptop computer equipped with an Intel i5-12500H processor and 16 GB of RAM. The decoupled models are solved using the IPOPT solver implemented on a general algebraic modeling system (GAMS) platform.

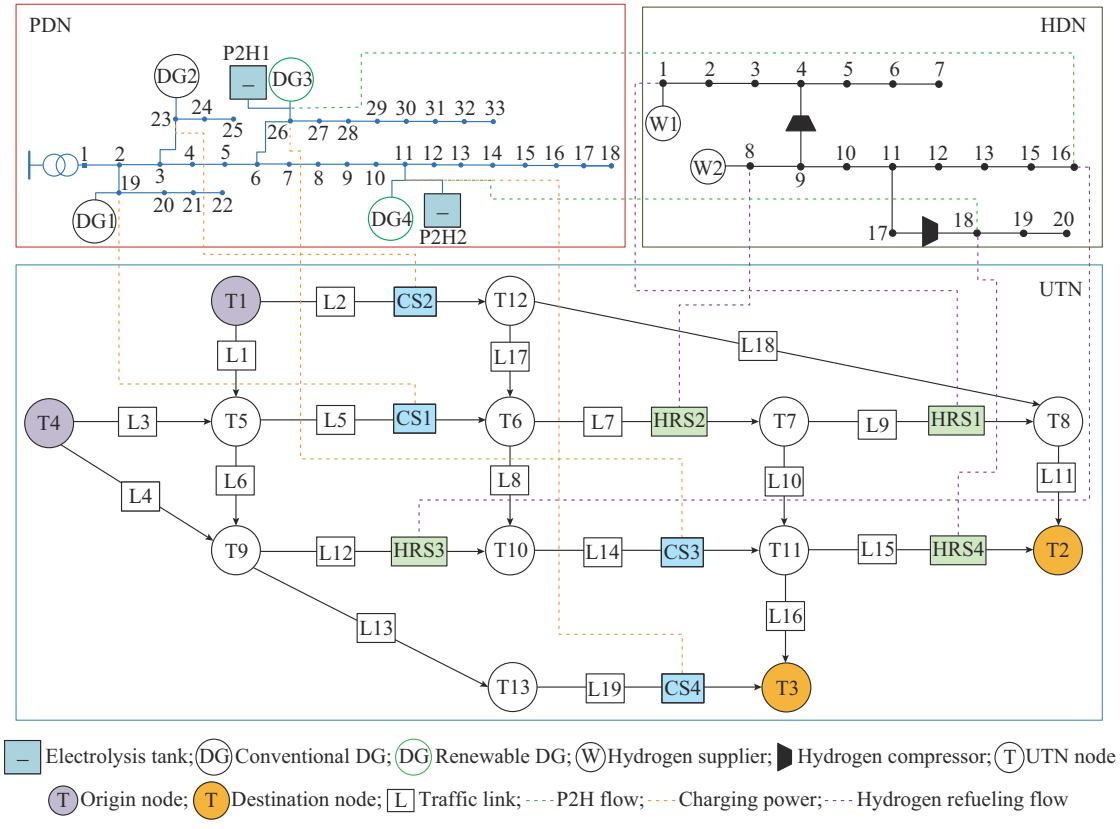


Fig. 4. Topology of coupled system.

We establish a DNN consisting of three hidden layers. To train and test the DNN, we extract the hourly load ratio variation data recorded for the 3rd, 6th, 8th, and 12th months of an 8760-hour dataset [34]. These data are employed to establish the electrical loads at the 33 nodes of PDN. The traffic demands for the four O-D pairs of UTN and the loads at the 20 nodes of HDN vary randomly from 80% to 100%. Employing GAMS to collaboratively optimize the three networks produce a dataset consisting of 8385 entries, which were divided into training and test datasets at the ratios of 80% and 20%, respectively. The DNN is implemented, trained, and tested using the PyTorch open-source machine

learning framework in Python 3.6.

### *A. Comparison of Differentiated and Non-differentiated Pricing Mechanisms*

We evaluate the performance of the proposed differentiated pricing mechanism in scheduling a heterogeneous fleet comprising EVs and HFCVs along with its advantages in reducing user travel costs. We first investigate the congestion tolls imposed on various regular links under differentiated and non-differentiated pricing mechanisms in the economically optimal conditions of tri-network coordinated operation. As shown in Fig. 5, as EVs constitute 70% of the heterogeneous vehicle fleet, the congestion tolls under the non-differentiated pricing mechanism are primarily driven by EVs, with charges closely aligned with those under the differentiated pricing mechanism. However, because of different locations of HRSs and CSs in the UTN, if HFCVs are subjected to the congestion pricing guidance designed for EVs, the result would be a "collective punishment" on the HFCV fleet, which would in turn reduce the economic efficiency of the network scheduling. The differentiated pricing mechanism mitigates these drawbacks by imposing separate congestion tolls on EVs and HFCVs. The results shown in Fig. 5 indicate that HFCVs are guided to refuel at HRS1 and HRS2 with lower congestion tolls on links L7 and L9, as these HRSs are supplied directly by hydrogen sources with minimal HDN losses. The pricing logic for EVs follows a similar rationale, even though EVs primarily serve the PDN. Overall, the tri-network coordinated operation achieves global optimization through the flexible scheduling of EVs and HFCVs.

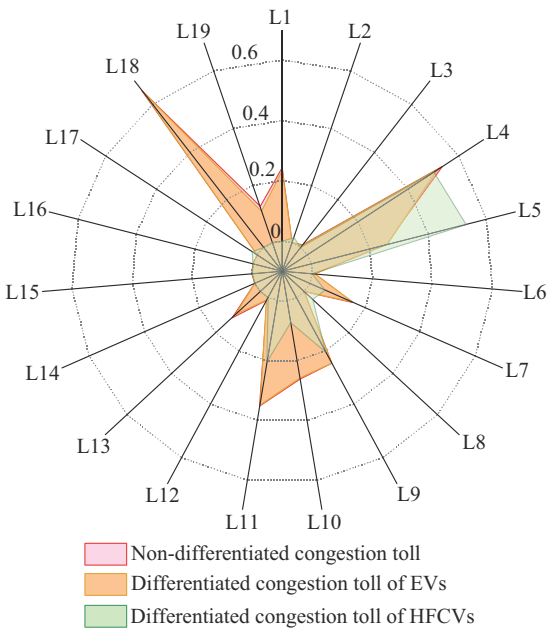


Fig. 5. Congestion tolls under different pricing mechanisms.

Furthermore, we investigate the traffic flow distribution in the UTN under different pricing mechanisms. Figure 6 presents the 3D color-mapped surface of the traffic flow distribution in the UTN under different pricing mechanisms. It is obvious that the road capacities of different regular links vary. Therefore, a uniform distribution of traffic flow in the UTN is not necessarily advantageous. The optimal strategy involves allocating traffic based on road capacities and directing more vehicles to segments with higher capacities and that are less susceptible to congestion. For example, the results shown in Fig. 6 indicate that the differentiated pricing mechanism enables links L1, L4, and L7, which have higher traffic capacities, to capture more flow, while simultaneously alleviating congestion on links L2, L3, and L5, which have lower traffic capacities. This more efficient pricing mechanism ultimately results in a reduction in user travel costs by approximately 1.3%.

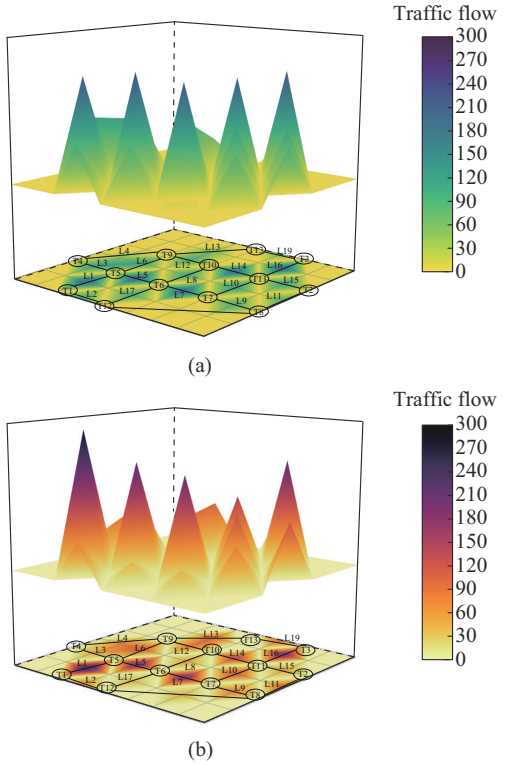


Fig. 6. Traffic flow distribution under different pricing mechanisms. (a) Non-differentiated pricing mechanism. (b) Differentiated pricing mechanism.

### *B. Performance of Proposed Learning-aided Approach*

#### *1) Bayesian Hyperparameter Tuning*

The hyperparameters of the established DNN subject to Bayesian hyperparameter tuning comprise the number of neurons in each of the three hidden layers as well as the learning rate and batch size. The tuning framework includes neuron counts in the hidden layers 1-3 in the integer ranges of [64, 256], [256, 1024], and [64, 256], respectively. The learning rate is evaluated over a logarithmic range of [0.0001, 0.1], and the batch size is evaluated with three commonly employed values of 32, 64, and 128.

Table I lists the initial hyperparameters and hyperparameters obtained after tuning. Notably, the tuning process significantly increases the $R^2$ value from 0.74 to 0.91, which represents a substantial enhancement of the fitting capabilities of the DNN. Figure 7 shows the evolution of the loss values obtained for the training and test datasets under an increas-

ing number of epochs. As shown in Fig. 7, the training and test loss values converge to approximately 0.02 before tuning. After tuning, these losses converge to approximately 0.015 and 0.005, respectively. Clearly, the prediction performance of the DNN is enhanced after tuning.

TABLE I
COMPARISON OF INITIAL HYPERPARAMETERS AND HYPERPARAMETERS OBTAINED AFTER TUNING

| Hyperparameter | Neurons of hidden layer 1 | Neurons of hidden layer 2 | Neurons of hidden layer 3 | Learning rate | Batch size | $R^2$ value |
|---|---|---|---|---|---|---|
| Initial | 150 | 600 | 200 | 0.05000 | 32 | 0.74 |
| After tuning | 140 | 566 | 252 | 0.00546 | 64 | 0.91 |

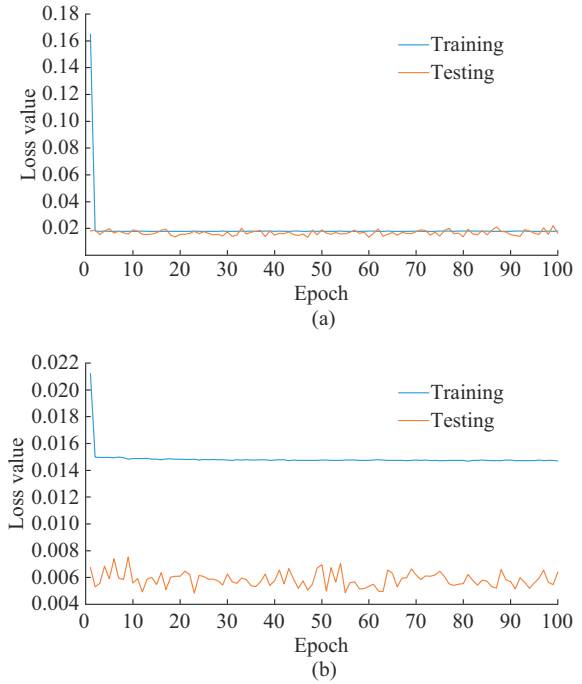


Fig. 7. Comparison of loss values obtained before and after tuning. (a) Before tuning. (b) After tuning.

*2) Comparison with Solutions Obtained by Directly Solving Coupled Physical Models*

We first compare the computational time between directly solving the coupled physical models of the PDN, HDN, and UTN using the sample data in the test dataset and the proposed learning-aided approach, as shown in Table II. The proposed learning-aided approach, which decouples the three networks and optimizes them separately based on hydrogen consumption and power demands as predicted by the trained DNN, reduces the required total time by 96.66% from 212.11 to 7.09 s. In addition, directly solving the coupled models yields the highest accuracy. We compare the operational costs of the PDN, HDN, and UTN obtained by directly solving the coupled physical models with those obtained by the proposed learning-aided approach based on the maximum relative error observed for the PDN, HDN, and UTN in the test dataset. The proposed learning-aided approach clearly obtains the highest scheduling accuracy for the PDN, with the maximum relative error rate of 0.11%. In addition, the inherent complexity and numerous nonlinear terms of the UTN results in the lowest scheduling accuracy, with the maximum relative error rate of 0.79%. In summary, the maximum relative error rate remains less than 0.8% for all the three networks and the combined system.

TABLE II
COMPARISON OF COMPUTATIONAL TIME BETWEEN DIRECTLY SOLVING COUPLED PHYSICAL MODEL AND PROPOSED LEARNING-AIDED APPROACH

| Approach | PDN time (s) | HDN time (s) | UTN time (s) | Prediction time (s) | Total time (s) |
|---|---|---|---|---|---|
| Directly solving | | | | | 212.11 |
| Proposed | 0.25 | 0.17 | 2.32 | 4.35 | 7.09 |

Compared with PDN, HDN exhibits more complex characteristics, which leads to greater difficulties in calculating the hydrogen consumption of HRSs and the power demand for hydrogen production, and brings greater differences in optimization costs. In addition, the proposed learning-aided approach relies on DNNs to predict coupled variables. If not properly accounted for, any inaccuracies in these predictions can lead to suboptimal HDN operations and increased costs. These findings demonstrate that the proposed learning-aided approach retains the economic advantages of collaborative optimization, even though the scheduling of each network is solved independently. This approach also significantly enhances the computational efficiency. Although the proposed learning-aided approach exhibits strong performance under normal operating conditions, its adaptability must be addressed under constraints such as power line overloads and voltage violations. To address these abnormal conditions, the proposed learning-aided approach requires regular retraining of the DNN using a more extensive dataset that includes cases that violate constraints. In addition, it is necessary to employ centralized optimization methods to coordinate solutions when dealing with these issues. This ensures that the proposed collaborative optimization framework remains effective with operational abnormalities.

*3) Operation Results from Model-driven Centralized Approach and Learning-aided Decomposed Approach*

We compare the dispatch solutions by directly solving the coupled physical models of the PDN, HDN, and UTN (model-driven approach) and the proposed learning-aided approach. Figure 8 compares the scheduling results for the PDN and HDN, and Fig. 9 shows the EV and HFCV distributions obtained at the CSs and HRSs in the UTN, respectively, under the two approaches. It is evident that the scheduling of the three networks is remarkably similar under the two approaches. For example, both approaches fully utilize the zero-cost photovoltaic outputs of DG3 and DG4. In addition, the relatively high cost of DG2, i.e., 49.41 $/MWh, results in a lower utilization rate than DG1 with a lower cost of 39.22 $/MWh. In fact, DG2 remains completely inactive under the model-driven approach, whereas the proposed learning-aided approach takes the power generated by DG2 to replace some of the power purchased from the main power grid at a similar cost of 47.51 $/MWh, which has only a

minor impact on the PDN operation cost. Similarly, the topological structure of the HDN and its compressor configuration, as shown in Fig. 4, make hydrogen supplier W2 bear a greater hydrogen demand than hydrogen supplier W1 under both approaches, even though the cost coefficient of hydrogen supplier W1 (i.e., 5 $/kcf) is less than that of hydrogen supplier W2 (i.e., 6 $/kcf).

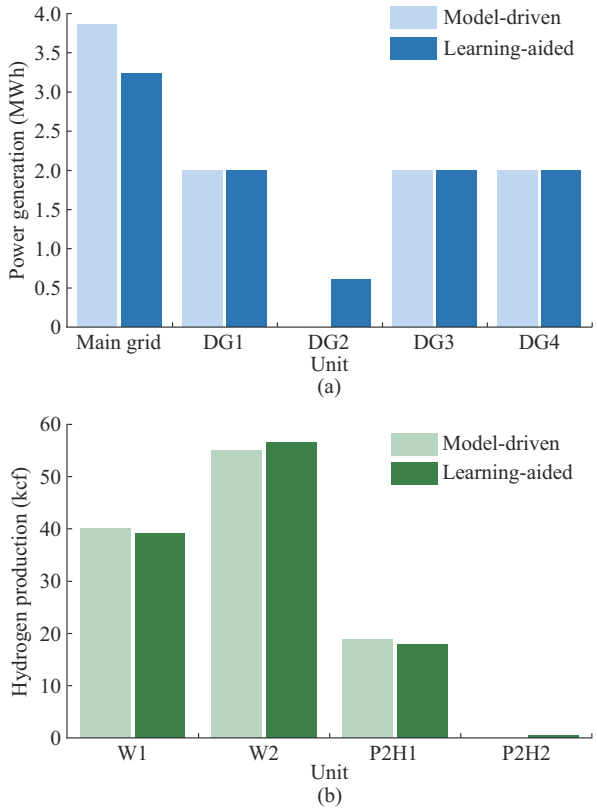


Fig. 8. Comparison of scheduling results for PDN and HDN. (a) Power generation. (b) Hydrogen production.

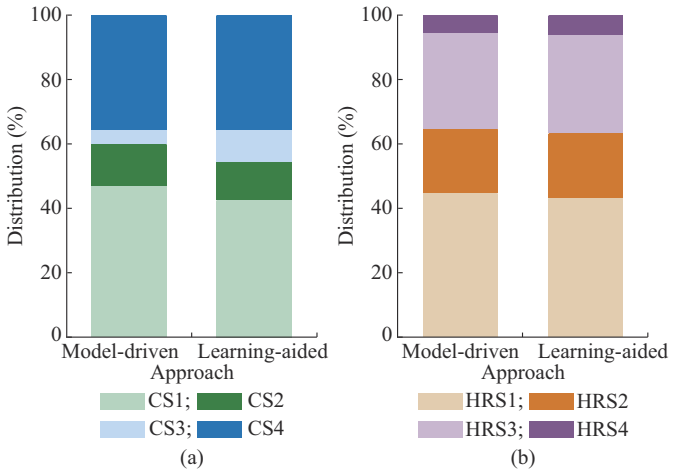


Fig. 9. Comparison of EV and HFCV distributions obtained at CSs and HRSs. (a) EV distribution. (b) HFCV distribution.

The results in Figs. 8 and 9 show that DG3 primarily supplies power to P2H1, whereas the minimum hydrogen production in P2H2 draws little power from DG4. Consequently, much less hydrogen is dispatched to HRS4 than to HRS3. By contrast, DG4 mainly powers CS4, which results in more EVs dispatched to CS4 than to CS3, thus ensuring that the output of photovoltaic resources is fully consumed. Regarding the dispatch of conventional units DG1 and DG2, we observe that more EVs are dispatched to CS1 than to CS2 due to the lower electricity cost from DG1 than that from DG2. Similarly, more HFCVs are dispatched to HRS1 than to HRS2 due to the lower hydrogen cost from hydrogen supplier W1 than that from hydrogen supplier W2. This effectively demonstrates the spatial responsiveness of the dispatching solutions to EV and HFCV traffic flows.

*4) Effects of Renewable DG Output Levels on Collaborative Optimization Results*

The renewable DG output levels directly influence the hydrogen output of the P2H units and the distribution of EVs and HFCVs at the CSs and HRSs, respectively. Therefore, we evaluate the dispatch solutions and P2H flow obtained using the proposed learning-aided approach under different renewable DG output levels of 0.5, 1, and 2 MW, as shown in Fig. 10.

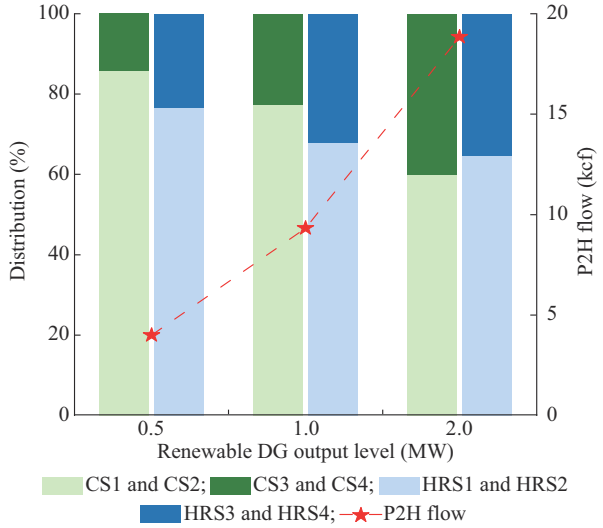


Fig. 10. Comparison of EV and HFCV distributions and P2H flow obtained under different renewable DG output levels.

As the renewable DG output level increases, the full consumption of renewable energy sources is supported by dispatching an increasing proportion of electricity and hydrogen from DG3 and DG4 to CS3, CS4, HRS3, and HRS4. In addition, the P2H flow steadily increases with the increasing renewable DG output levels. This indicates that the P2H technology plays a significant role in ensuring full consumption of renewable energy sources.

*5) Effects of Hydrogen Loads on HFCV Distributions*

We also evaluate the dispatch solutions obtained using the proposed learning-aided approach with hydrogen load factors of 0.9, 1.0, 1.1, and 1.2, as shown in Fig. 11. The hydrogen supply dispatched to HRS1 and HRS2 notably increases with the hydrogen load factor. By contrast, the hydrogen supply dispatched to HRS3 and HRS4 gradually decreases.

These results can be attributed to the inherent losses in hydrogen transport in the HDN, which increases as the HDN

becomes more heavily loaded. Therefore, the dispatch solutions obtained with increasing hydrogen load factors may mitigate losses to some extent by increasing the proportion of hydrogen directly dispatched from hydrogen suppliers W1 and W2 located at nodes 1 and 8 of the HDN, respectively.

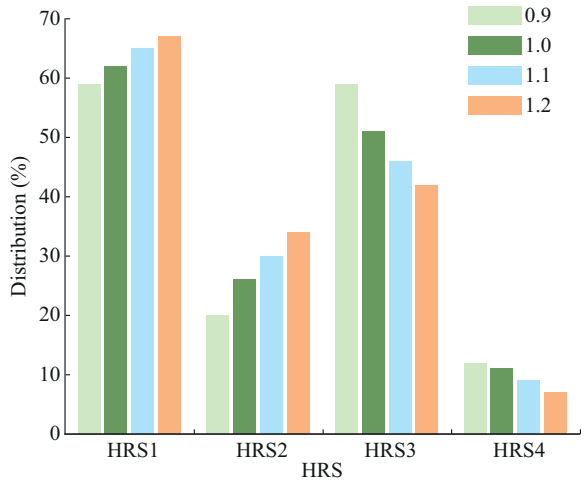


Fig. 11. Comparison of HFCV distributions at different HRSs under various hydrogen load factors.

## V. Conclusion

This study develops a coordinated optimization model for a power-hydrogen-transportation network and employs a differentiated taxation-subsidy mechanism to guide EVs and HFCVs more effectively, thereby facilitating the coordinated operation of the UTN with the PDN and UTN while reducing user travel costs by approximately 1.3%. This study also addresses significant limitations in current efforts to coordinate the operations of coupled PDN, HDN, and UTN by proposing a learning-aided approach. Applying the predicted values capitalizes on the economic benefits of joint optimization and enables the networks to be decoupled, thereby enabling them to operate and be optimized independently. This greatly simplifies the optimization process, restricting the exchange of private information between the three network operators and eliminating the requirement of operators to have specific information regarding the operations of all three networks. Given the nonlinear complexity of the physical system models, Bayesian hyperparameter tuning is applied to determine the optimal hyperparameters of DNN, which improves its prediction performance. The results of numerical simulations of a coupled system composed of an IEEE 33-node power network, 13-node Nguyen-Dupuis transportation network, and 20-node HDN demonstrates that the dispatching results yielded by the proposed learning-aided approach differ from those by the model-driven approach by less than 1% while improving the computational efficiency by more than 96%.

This study is important for the application of learning machine approaches in improving the computational efficiency of traditional large-scale optimization models of energy systems. In addition, the information privacy of multi-energy networks is preserved by learning the coupling power information, which contributes to a sufficiently coordinated solution while maintaining the existing operational independence of each energy system. Notably, the data-driven approaches have limitations in terms of data quality, availability, and the possibility of model overfitting. To address these limitations, we incorporate strategies such as rigorous data preprocessing to ensure quality and regularization techniques within the DNN to prevent overfitting.

This study focuses on static PDN, HDN, and UTN models. In the future work, we hope to explore the dynamic versions of these networks while considering the potential integration of physical or graph neural networks. For a dynamic version, we suggest incorporating a temporal discretization approach into the model to allow it to capture the dynamic evolution of network states. In addition, we suggest implementing a rolling-horizon optimization strategy coupled with event-triggered updates to ensure the computational efficiency and to redirect the focus on critical decision-making moments.

## References

[1] A. Hajebrahimi, I. Kamwa, E. Delage *et al*., "Adaptive distributionally robust optimization for electricity and electrified transportation planning," *IEEE Transactions on Smart Grid*, vol. 11, no. 5, pp. 4278-4289, Sept. 2020.

[2] H. Patil and V. N. Kalkhambkar, "Grid integration of electric vehicles for economic benefits: a review," *Journal of Modern Power Systems and Clean Energy*, vol. 9, no. 1, pp. 13-26, Jan. 2021.

[3] G. Pan, W. Gu, Y. Lu *et al*., "Optimal planning for electricity-hydrogen integrated energy system considering power to hydrogen and heat and seasonal storage," *IEEE Transactions on Sustainable Energy*, vol. 11, no. 4, pp. 2662-2676, Oct. 2020.

[4] K. Zhang, B. Zhou, S. W. Or *et al*., "Optimal coordinated control of multi-renewable-to-hydrogen production system for hydrogen fueling stations," *IEEE Transactions on Industry Applications*, vol. 58, no. 2, pp. 2728-2739, Mar. 2022.

[5] Z. Jia, J. Li, X. P. Zhang *et al*., "Review on optimization of forecasting and coordination strategies for electric vehicle charging," *Journal of Modern Power Systems and Clean Energy*, vol. 11, no. 2, pp. 389-400, Mar. 2023.

[6] G. Sun, G. Li, P. Li *et al*., "Coordinated operation of hydrogen-integrated urban transportation and power distribution networks considering fuel cell electric vehicles," *IEEE Transactions on Industry Applications*, vol. 58, no. 2, pp. 2652-2665, Mar. 2022.

[7] X. Wu, H. Li, X. Wang *et al*., "Cooperative operation for wind turbines and hydrogen fueling stations with on-site hydrogen production," *IEEE Transactions on Sustainable Energy*, vol. 11, no. 4, pp. 2775-2789, Oct. 2020.

[8] S. Lv, S. Chen, Z. Wei *et al*., "Power-transportation coordination: toward a hybrid economic-emission dispatch model," *IEEE Transactions on Power Systems*, vol. 37, no. 5, pp. 3969-3981, Sept. 2022.

[9] S. Xie, Q. Wu, N. D. Hatziargyriou *et al*., "Collaborative pricing in a power-transportation coupled network: a variational inequality approach," *IEEE Transactions on Power Systems*, vol. 38, no. 1, pp. 783-795, Jan. 2023.

[10] C. Shao, K. Li, X. Li *et al*., "A decentralized bi-level decomposition method for optimal operation of electric vehicles in coupled urban transportation and power distribution systems," *IEEE Transactions on Transportation Electrification*, vol. 10, no. 1, pp. 2235-2246, Mar. 2024.

[11] H. Fan, D. Wang, Z. Yu *et al*., "Bilevel optimal scheduling of electric bus fleets in regional integrated electricity-gas-heat energy systems," *IEEE Transactions on Transportation Electrification*, vol. 9, no. 2, pp. 2792-2807, Jun. 2023.

[12] Z. Shi, Y. Xu, D. Xie *et al*., "Optimal coordination of transportable power sources and repair crews for service restoration of distribution networks considering uncertainty of traffic congestion," *Journal of Modern Power Systems and Clean Energy*, vol. 12, no. 1, pp. 189-201, Jan. 2024.

[13] W. Dong, C. Shao, C. Feng *et al*., "Cooperative operation of power and hydrogen energy systems with HFCV demand response," *IEEE*

*Transactions on Industry Applications*, vol. 58, no. 2, pp. 2630-2639, Mar. 2022.
[14] Y. Tao, J. Qiu, S. Lai *et al*., "Coordinated planning of electricity and hydrogen networks with hydrogen supply chain for fuel cell electric vehicles," *IEEE Transactions on Sustainable Energy*, vol. 14, no. 2, pp. 1010-1023, Apr. 2023.
[15] Y. Liang, Z. Ding, T. Ding *et al*., "Mobility-aware charging scheduling for shared on-demand electric vehicle fleet using deep reinforcement learning," *IEEE Transactions on Smart Grid*, vol. 12, no. 2, pp. 1380-1393, Mar. 2021.
[16] Z. Zhao and C. K. M. Lee, "Dynamic pricing for EV charging stations: a deep reinforcement learning approach," *IEEE Transactions on Transportation Electrification*, vol. 8, no. 2, pp. 2456-2468, Jun. 2022.
[17] T. Qian, C. Shao, X. Li *et al*., "Multi-agent deep reinforcement learning method for EV charging station game," *IEEE Transactions on Power Systems*, vol. 37, no. 3, pp. 1682-1694, May 2022.
[18] Q. Yuan, Y. Ye, Y. Tang *et al*., "A novel deep-learning based surrogate modeling of stochastic electric vehicle traffic user equilibrium in low-carbon electricity-transportation nexus," *Applied Energy*, vol. 315, p. 118961, Jun. 2022.
[19] L. Cui, Q. Wang, H. Qu *et al*., "Dynamic pricing for fast charging stations with deep reinforcement learning," *Applied Energy*, vol. 346, p. 121334, Sept. 2023.
[20] K. Wang, H. Wang, Z. Yang *et al*., "Analysis of coordinated operation of power-transportation systems based on multi-objective optimization, " *Applied Energy*, vol. 343, p. 121186, Aug. 2023.
[21] T. Qian, C. Shao, X. Wang *et al*., "Deep reinforcement learning for EV charging navigation by coordinating smart grid and intelligent transportation system," *IEEE Transactions on Smart Grid*, vol. 11, no. 2, pp. 1714-1723, Mar. 2020.
[22] K. Park and I. Moon, "Multi-agent deep reinforcement learning approach for EV charging scheduling in a smart grid," *Applied Energy*, vol. 328, p. 120111, Dec. 2022.
[23] B. Li, J. Li, and M. Han, "Deep reinforcement learning-based charging price determination considering the coordinated operation of hydrogen fuel cell electric vehicle, power network and transportation network," *IEEE Access*, vol. 11, pp. 75508-75521, Jul. 2023.
[24] W. Wei, L. Wu, J. Wang *et al*., "Network equilibrium of coupled transportation and power distribution systems," *IEEE Transactions on Smart Grid*, vol. 9, no. 6, pp. 6764-6779, Nov. 2018.
[25] J. Munoz, N. Jimenez-Redondo, J. Perez-Ruiz *et al*., "Natural gas network modeling for power systems reliability studies," in *Proceedings of 2003 IEEE Bologna Power Tech Conference Proceedings*, Bologna, Italy, Jun. 2023, pp. 1-4.
[26] S. Chen, A. J. Conejo, R. Sioshansi *et al*., "Unit commitment with an enhanced natural gas-flow model," *IEEE Transactions on Power Systems*, vol. 34, no. 5, pp. 3729-3738, Sept. 2019.
[27] M. Farivar and S. H. Low, "Branch flow model: relaxations and convexification—part I," *IEEE Transactions on Power Systems*, vol. 28, no. 3, pp. 2554-2564, Aug. 2013.
[28] M. Farivar and S. H. Low, "Branch flow model: relaxations and convexification—part II," *IEEE Transactions on Power Systems*, vol. 28, no. 3, pp. 2565-2572, Aug. 2013.
[29] G. P. Meyer, "An alternative probabilistic interpretation of the Huber loss," in *Proceedings of 2021 IEEE/CVF Conference on Computer Vision and Pattern Recognition* (*CVPR*), Nashville, USA, Jun. 2021, pp. 5257-5265.
[30] V. Nguyen, "Bayesian optimization for accelerating hyper-parameter tuning," in *Proceedings of 2019 IEEE Second International Conference on Artificial Intelligence and Knowledge Engineering* (*AIKE*), Sardinia, Italy, Jun. 2019, pp. 302-305.
[31] M. E. Baran and F. F. Wu, "Optimal capacitor placement on radial distribution systems," *IEEE Transactions on Power Delivery*, vol. 4, no. 1, pp. 725-734, Jan. 1989.
[32] S. Nguyen and C. Dupuis, "An efficient method for computing traffic equilibria in networks with asymmetric transportation costs," *Transportation Science*, vol. 18, no. 2, pp. 185-202, May 1984.
[33] S. Chen, G. Sun, Z. Wei *et al*., "Dynamic pricing in electricity and natural gas distribution networks: an EPEC model," *Energy*, vol. 207, p. 118138, Sept. 2020.
[34] I. Pena, C. B. Martinez-Anido, and B.-M. Hodge, "An extended IEEE 118-bus test system with high renewable penetration," *IEEE Transactions on Power System*, vol. 33, no. 1, pp. 281-289, Jan. 2018.

**Sheng Chen** received the B.S. and Ph.D. degrees from the School of Electrical and Power Engineering, Hohai University, Nanjing, China, in 2014 and 2019, respectively. From January 2018 to January 2019, he was a Visiting Scholar at The Ohio State University, Columbus, USA. He is currently a Professor with the School of Electrical and Power Engineering, Hohai University. His research interests include integrated energy system, operation research, and electricity market.

**Hao Cheng** received the B.S. degree from the School of Electrical and Information Engineering, Jiangsu University, Zhenjiang, China, in 2022. He is currently pursuing the M.S. degree from the School of Electrical and Power Engineering, Hohai University, Nanjing, China. His research interests include coordinated operation of intelligent power and transportation system.

**Si Lv** received the B.S. and Ph.D. degrees from the School of Electrical and Power Engineering, Hohai University, Nanjing, China, in 2018 and 2024, respectively. From June 2022 to June 2023, he was a Visiting Scholar at the Department of Energy Technology, Aalborg University, Aalborg, Denmark. His research interests include coordinated planning & operation of interdependent power and transportation system.

**Zhinong Wei** received the B.S. degree from Hefei University of Technology, Hefei, China, in 1984, the M.S. degree from Southeast University, Nanjing, China, in 1987, and the Ph.D. degree from Hohai University, Nanjing, China, in 2004. He is currently a Professor of electrical engineering with the School of Electrical and Power Engineering, Hohai University. His research interests include integrated energy system, power system state estimation, smart distribution system, and integration of distributed generation into electric power system.

**Peiyue Li** received the B.S. degree from the School of Electrical and Control Engineering, North University of China, Taiyuan, China, in 2019, and the M.S. degree from the School of Electrical and Engineering, Shanghai DianJi University, Shanghai, China, in 2023. She is currently pursuing the Ph. D. degree from the School of Electrical and Power Engineering, Hohai University, Nanjing, China. Her research interests include coordinated operation of intelligent power and transportation system.

**Jiahui Jin** received the B.S. degree from the School of Electrical and Engineering, Southwest Jiaotong University, Chengdu, China, in 2019, and the M.S. degree from the School of Electrical and Engineering, Shanghai DianJi University, Shanghai, China, in 2023. He is currently pursuing the Ph.D. degree from the School of Electrical and Power Engineering, Hohai University, Nanjing, China. His research interests include coordinated operation of intelligent power distribution network and microgrid.